Table 1 **Calculated Helmholtz free energy of the b.c.c. and h.c.p. phases of Fe**

Volume (Å^3)	Temperature (K)	$F_{b.c.c.}$ (eV)	$F_{h.c.p.}$ (eV)	$\Delta F_{b.c.c.-h.c.p.}$ (meV)
9.0	3,500	−10.063	−10.109	46
8.5	3,500	− 9.738	− 9.796	58
7.8	5,000	−10.512	−10.562	50
7.2	6,000	−10.633	−10.668	35
6.9	6,500	−10.545	−10.582	37
6.7	6,700	−10.288	−10.321	33
*7.2	3,000	− 7.757	− 7.932	175

Shown is the *ab initio* Helmholtz free energy per atom of the b.c.c. and h.c.p. phases of Fe, $F_{b.c.c.}$ and $F_{h.c.p.}$, at state points along (*and below) the calculated melting curve[23]. In this work, the reference system is a simple inverse power potential which takes the form $U = 4\varepsilon(\Gamma/r)^\alpha$ where $\varepsilon = 1$ eV, $\Gamma = 1.77$ Å, $\alpha = 5.86$. We have previously shown that this reference potential, based on only a repulsive term, describes the *ab initio* system extremely well; the bonding term is almost independent of the atomic positions, depending only on the volume and temperature of the system[21,24]. We stress, however, that the final result is totally independent of the choice of reference system. We performed these calculations on a 64-atom supercell ($4 \times 4 \times 4$ primitive cells) with a $3 \times 3 \times 3$ **k**-point grid. Considerable effort was spent on convergence tests in **k**-point sampling to reduce the error in free energies to <10 meV per atom. Cell size effects have been extensively studied in our previous work on h.c.p.-Fe[21].

known not to be made of pure Fe, but is expected to be alloyed with between 5 to 10 mol.% of a lighter element. It is now reasonably well established that either separately or together S and Si are two of the most probable light elements alloyed with Fe in the core[26–29]. Additionally, recent experiments[30] have shown that at high pressures FeSi crystallizes with the CsCl-structure (that is, has identical atomic coordinates to b.c.c.-Fe), and at lower concentrations Si stabilizes b.c.c.-Fe under pressure and temperature conditions at which pure Fe is found with the h.c.p. structure[26]. We therefore investigated the energetic effect of the substitution of S and Si in b.c.c. and h.c.p.-Fe at representative core cell volumes (7.2 Å^3). We find that the enthalpies of the S and Si defects are respectively 1.4 and 1.2 eV per defect atom more stable in the b.c.c. structure than in the h.c.p. phase. Therefore, for example, a 5 mol.% concentration of Si in Fe, would stabilize the b.c.c. phase by 60 meV. Thus, in contrast with lower-pressure experiments[26], we conclude that the presence of S or Si as the light impurity element in the core, at appropriate concentrations, could favour the formation of a b.c.c.- rather than an h.c.p.-structured Fe alloy phase at temperatures just below T_m at inner core pressure.

In contrast to earlier work, we have shown that a b.c.c.-structured phase is entropically stabilized under inner core conditions, and is made more stable than the h.c.p.-phase by impurities in the inner core. This means that a b.c.c.-structured alloy is a strong candidate for explaining the recently observed[2–4] seismic complexity of the inner core. □

Received 21 August 2002; accepted 18 June 2003; doi:10.1038/nature01829.

1. Brown, M. J. The equation of state of iron to 450 GPa: Another high-pressure solid phase? *Geophys. Res. Lett.* **28,** 4339–4342 (2001).
2. Song, X. D. & Helmberger, D. V. Seismic evidence for an inner core transition zone. *Science* **282,** 924–927 (1998).
3. Beghein, C. & Trampert, J. Robust normal mode constraints on inner-core anisotropy from model space search. *Science* **299,** 552–555 (2003).
4. Ishii, M. & Dziewonski, A. M. The innermost inner core of the earth: Evidence for a change in anisotropic behavior at the radius of about 300 km. *Proc. Natl Acad. Sci. USA* **99,** 14026–14030 (2002).
5. Steinle-Neumann, G., Stixrude, L., Cohen, R. E. & Gülseren, O. Elasticity of iron at the temperature of the Earth's inner core. *Nature* **413,** 57–60 (2001).
6. Vočadlo, L., Brodholt, J., Alfè, D., Gillan, M. J. & Price, G. D. Ab initio free energy calculations on the polymorphs of iron at core conditions. *Phys. Earth Planet. Inter.* **117,** 123–137 (2000).
7. Shen, G. Y., Mao, H. K., Hemley, R. J., Duffy, T. S. & Rivers, M. L. Melting and crystal structure of iron at high pressures and temperatures. *Geophys. Res. Lett.* **25,** 373–376 (1998).
8. Ross, M., Young, D. A. & Grover, R. Theory of the iron phase diagram at Earth core conditions. *J. Geophys. Res.* **95,** 21713–21716 (1990).
9. Matsui, M. & Anderson, O. L. The case for a body-centred-cubic phase (α') for iron at inner core conditions. *Phys. Earth Planet Inter.* **103,** 55–62 (1997).
10. Petry, W. Dynamical precursors of martensitic transitions. *J. Phys. IV* **5,** C2-15–C2-28 (1995).
11. Trampenau, J. *et al.* Phonon dispersion of the bcc phase of group-IV metals. III. bcc hafnium. *Phys. Rev. B* **43,** 10963–10969 (1991).
12. Söderlind, P., Moriarty, J. A. & Willis, J. M. First-principles theory of iron up to Earth-core pressures: structural, vibrational and elastic properties. *Phys. Rev. B* **53,** 14063–14072 (1996).
13. Stixrude, L. & Cohen, R. E. Constraints on the crystalline structure of the inner core: mechanical instability of BCC iron at high pressures. *Geophys. Res. Lett.* **22,** 125–128 (1995).
14. Moriarty, J. A. in *High Pressure Science and Technology 1993* (eds Schmidt, S. C., Shaner, J. W., Samara, G. A. & Ross, M.) 233–236 (AIP Press, New York, 1994).
15. Mao, H. K. *et al.* Phonon density of states of iron up to 153 gigapascals. *Science* **292,** 914–916 (2001).
16. Hohenberg, P. & Kohn, W. Inhomogeneous electron gas. *Phys. Rev.* **136,** B864–B871 (1964).
17. Wang, Y. & Perdew, J. Correlation hole of the spin-polarized electron gas, with exact small-wave-vector and high-density scaling. *Phys. Rev. B* **44,** 13298–13307 (1991).
18. Kresse, G. & Furthmüller, J. Efficient iterative schemes for *ab initio* total-energy calculations using a plane-wave basis set. *Phys. Rev. B* **54,** 11169–11186 (1996).
19. Blöchl, P. E. Projector augmented-wave method. *Phys. Rev. B* **50,** 17953–17979 (1994).
20. Alfè, D., Kresse, G. & Gillan, M. J. Structure and dynamics of liquid iron under Earth's core conditions. *Phys. Rev. B* **61,** 132–142 (2000).
21. Alfè, D., Price, G. D. & Gillan, M. J. Thermodynamics of hexagonal-close-packed iron under Earth's core conditions. *Phys. Rev. B* **64,** 045123 (2001).
22. Grad, G. B. *et al.* Electronic structure and chemical bonding effects upon the bcc to Ω phase transition: *ab initio* study of Y, Zr, Nb and Mo. *Phys. Rev. B* **62,** 12743–12753 (2000).
23. Alfè, D., Gillan, M. J. & Price, G. D. The melting curve of iron at Earth's core pressures from *ab initio* calculations. *Nature* **401,** 462–464 (1999).
24. Alfè, D., Price, G. D. & Gillan, M. J. Iron under Earth's core conditions: liquid-state thermodynamics and high pressure melting curve from *ab initio* calculations. *Phys. Rev. B* **65,** 165118 (2002).
25. Vočadlo, L. & Alfè, D. *Ab initio* melting curve of the *fcc* phase of aluminium. *Phys. Rev. B* **65,** 214105 (2002).
26. Lin, J.-F., Heinz, D. L., Campbell, A. J., Devine, J. M. & Shen, G. Iron-silicon alloy in Earth's core? *Science* **295,** 313–315 (2002).
27. Alfè, D., Price, G. D. & Gillan, M. J. Composition and temperature of the Earth's core constrained by combining ab initio calculations and seismic data. *Earth Planet. Sci. Lett.* **195,** 91–98 (2002).
28. Alfè, D., Price, G. D. & Gillan, M. J. *Ab initio* chemical potentials of solid and liquid solutions and the chemistry of the Earth's core. *J. Chem. Phys.* **116,** 7127–7136 (2002).
29. Alfè, D., Gillan, M. J. & Price, G. D. Constraints on the composition of the Earth's core from *ab-initio* calculations. *Nature* **405,** 172–175 (2000).
30. Dobson, D. P., Vočadlo, L. & Wood, I. G. A new high-pressure phase of FeSi. *Am. Mineral.* **87,** 784–787 (2002).

Acknowledgements L.V. and D.A. thank the Royal Society for their continued support through the University Fellowship scheme. We also thank NERC for providing computing facilities via grants.

Competing interests statement The authors declare that they have no competing financial interests.

Correspondence and requests for materials should be addressed to L.V. (l.vocadlo@ucl.ac.uk).

Measuring fast neutrons in Hiroshima at distances relevant to atomic-bomb survivors

T. Straume[1,2], G. Rugel[3,4], A. A. Marchetti[2], W. Rühm[4], G. Korschinek[3], J. E. McAninch[2], K. Carroll[2], S. Egbert[5], T. Faestermann[3], K. Knie[3], R. Martinelli[2], A. Wallner[3,4] & C. Wallner[3]

[1]*University of Utah, 729 Arapeen Drive, Suite 2334, Salt Lake City, Utah 84108, USA*
[2]*Lawrence Livermore National Laboratory (LLNL), PO Box 808, Livermore, California 94550, USA*
[3]*Technische Universität München, D-85747 Garching, Germany*
[4]*Ludwig Maximilians Universität München, D-80336, München, Germany*
[5]*Science Applications International Corporation, 10260 Campus Point Drive, San Diego, California 92121, USA*

Data from the survivors of the atomic bombs serve as the major basis for risk calculations of radiation-induced cancer in humans[1]. A controversy has existed for almost two decades, however, concerning the possibility that neutron doses in Hiroshima may have been much larger than estimated. This controversy was based on measurements of radioisotopes activated by thermal neutrons that suggested much higher fluences at larger distances than expected[2–6]. For fast neutrons, which contributed almost all the neutron dose, clear measurement validation has so far proved impossible at the large distances (900 to 1,500 m) most relevant to survivor locations[6]. Here, the first

results are reported for the detection of ^{63}Ni produced predominantly by fast neutrons (above about 1 MeV) in copper samples from Hiroshima. This breakthrough was made possible by the development of chemical extraction methods[7,8] and major improvements in the sensitivity of accelerator mass spectrometry for detection of ^{63}Ni atoms (refs 8–11). When results are compared with ^{63}Ni activation predicted by neutron doses for Hiroshima survivors[6], good agreement is observed at the distances most relevant to survivor data. These findings provide, for the first time, clear measurement validation of the neutron doses to survivors in Hiroshima.

It was recognized in the final report of the 1986 reassessment of the atomic bomb radiation dosimetry for Hiroshima and Nagasaki (DS86)[6] that the calculated neutron doses for survivors could possibly be wrong. The principal reasons for this concern were: (1) the observation that a large discrepancy was suggested between the available ^{60}Co activation measured in Hiroshima[12] and calculations based on DS86 and (2) the paucity of neutron validation measurements available at that time, preventing adequate resolution of this matter. It was concluded that the neutron doses are in doubt until further work is done and that special efforts should be made to provide additional neutron measurements[6]. This generated extensive interest and resulted in a large number of low-energy (thermal) neutron activation measurements in Hiroshima[2–5,13–18] and to a lesser extent in Nagasaki[19]. See the review of ref. 20 for a more complete list of thermal neutron references. Even with the additional thermal neutron measurements, a definitive determination of the neutron dose has not been possible because of factors such as uncertainties in the measured background and uncertainties in the relationships between thermal neutrons and neutron dose. In contrast, fast neutrons produced essentially all of the neutron dose in Hiroshima and are much less dependent on sample environment. Although fast neutron measurements (above about 2 MeV) were made in Hiroshima within weeks of the bombings by beta-ray counting of the radioisotope ^{32}P (half-life, 14.2 days) in sulphur samples[21–22], the results reached background levels[23] at about 700 m from the hypocentre (the point on the ground below the explosion). Hence, they could not be used for direct validation of fast neutrons at the larger distances most relevant for the data on atomic-bomb survivors. For these reasons, it is clear that fast-neutron activation measurements at relevant distances in Hiroshima would be indispensable for validation of the neutron doses received by atomic-bomb survivors.

We have developed the capability to detect trace amounts of ^{63}Ni (half-life, 100.1 ± 2.0 yr[24]) in copper using accelerator mass spectrometry (AMS)[7–11,25,26]. The amount of ^{63}Ni produced via the reaction ^{63}Cu(n,p)^{63}Ni in copper samples exposed to atomic-bomb neutrons is a measure of the fast-neutron fluence[25–27]. On the basis of the available cross-sections, 95% of the activation from this reaction was by neutrons above 1.5 MeV in Hiroshima. Quantitative extraction of 100 to 400 μg nickel, containing only a few million atoms of ^{63}Ni, was required from gram-sized copper samples. Stable ^{63}Cu (69% natural abundance) is an isobar to ^{63}Ni and causes severe interference in the mass spectrometric measurements. For example, Hiroshima samples beyond 1,000 m from the hypocentre were expected to contain 18 orders of magnitude more ^{63}Cu than ^{63}Ni. Thus, the nickel had to be chemically separated from copper before AMS analysis could take place. Methods were developed consisting of electrochemical separation to remove the gross copper material followed by a procedure in which the nickel reacted with carbon monoxide to form nickel tetracarbonyl, a volatile compound which could be thermally decomposed to nickel metal directly in the AMS sample holder. Both of these processes are highly specific to nickel. Details of the methods are given elsewhere[7,8]. Two laboratories were involved in the AMS measurements. At the Livermore facility, ^{63}Ni^{10+} ions were accelerated to 99 MeV and counted in a four-anode gas ionization detector; the overall system had a typical rejection factor of 5×10^5 for ^{63}Cu. At the Munich tandem laboratory, ^{63}Ni^{12+} ions were accelerated to 175 MeV. At this energy, a gas-filled magnet could be used to separate the isobars further. The use of a gas-filled magnet in combination with a position- and angle-sensitive multi-anode gas ionization detector resulted in a ^{63}Cu rejection factor of 10^9. The achievement of this high rejection factor for ^{63}Cu allowed measurements of distant samples and also of close samples high in stable nickel. Both systems have been described in more detail previously[8–11].

Suitable copper samples had to have: (1) a known location at the time of the bombing, (2) been in line-of-sight of the explosion with no or minimal intervening shielding, (3) been located at distances most relevant to the atomic-bomb survivor health studies, and (4) be low in stable nickel to keep the competing production from the thermal ^{62}Ni(n,γ)^{63}Ni reaction as low as possible and thereby maximize the ^{63}Ni/Ni ratio. Bomb-exposed copper samples have been collected from seven distances in Hiroshima ranging from 380 m to more than 5,000 m from the hypocentre. Each of these samples has been measured two or more times. The samples from 380 to 1,461 m provide direct information on the fast-neutron fluences while the samples from 1,880 and 5,062 m determine the

Table 1 **^{63}Ni activation in copper samples in Hiroshima**

Sample location (distance from hypocentre)	Description of samples	Number of measurements	^{63}Ni per g Cu measured ($\times 10^4$)	^{63}Ni per g Cu measured-background† ($\times 10^4$)	^{63}Ni per g Cu calculated‡ ($\times 10^4$)
Bank of Japan (380 m)	Lightning conductor, unshielded	3	400 ± 40	580 ± 50	904
Soy Sauce Brewery (949 m)	Lightning conductor, inside an iron pipe (0.35 cm Fe shielding)	2	44 ± 14	54 ± 20	50
City Hall (1,014 m)	Lightning conductor, inside an iron pipe (0.40 cm Fe shielding)	6	26.5 ± 2.7	28 ± 5	30
Elementary school (1,301 m)	Rain gutter, unshielded	3	11.0 ± 1.4	5.4 (+4.1, −3.4)	5.6
Radioisotope building (1,461 m)	Rain gutter, unshielded	3	10.3 ± 1.7	4.5 (+4.5, −3.8)	3.0
Sumitomo Bank§ (1,880 m)	Rain gutter, unshielded	2	7.3 (+2.6, −2.1)		
Kusatsu Hachiman Shrine§ (5,062 m)	Copper roof, unshielded	2	7 (+8, −5)		

Results of measured and calculated (DS86) ^{63}Ni activation (given numbers are rounded). The hypocentre is the location on the ground directly under the bomb explosion. According to DS86, the Hiroshima bomb was exploded at 580 m above the hypocentre. Each sample was measured two or more times. The City Hall sample was measured using both the LLNL and the Munich AMS facility. The others were measured using the Munich facility only.

*Uncertainties correspond to 68% confidence intervals for Poisson-distributed data[30].

† A background of 7.3×10^4 ^{63}Ni per g Cu was subtracted from the measured values and the results corrected for decay since 1945.

‡ ^{63}Ni per g Cu calculated to have been produced in each sample by Hiroshima bomb neutrons based on the DS86 neutron output and energy spectrum, including both ^{63}Cu(n,p)^{63}Ni and ^{62}Ni(n,γ)^{63}Ni reactions.

§ The weighted average of these two large-distance samples was used for background subtraction.

^{63}Ni content in copper samples not exposed significantly to bomb neutrons.

The calculations of the activation of ^{63}Ni in copper samples were based on the DS86[6] neutron output (angle and spectrum) and the DS86 aboveground fluences. The *in situ* sample calculations were performed using a Monte Carlo adjoint shielding code[28]. The calculations derived the number of ^{63}Ni atoms created in the copper sample by: (1) transporting local DS86 above ground fluences in air, sample, and surrounding materials taking into account scattering and absorption, and (2) taking into account the energy-dependence of the cross-sections[29] for the two relevant reactions, that is, ^{63}Cu(n,p)^{63}Ni (fast neutrons) and ^{62}Ni(n,γ)^{63}Ni (thermal neutrons). The fraction of ^{63}Ni produced by thermal neutrons in the copper samples was calculated to be 24% (380 m), 5.7% (949 m), 0.2% (1,014 m), 0.3% (1,301 m), and 0.1% (1,461 m), respectively.

The description of the Hiroshima copper samples and the measurement and calculation results are listed in Table 1. The measured results are expressed as mean ^{63}Ni atoms per g Cu values with uncertainties corresponding to 68% confidence intervals. The statistical uncertainty was obtained using a well-established procedure for Poisson-distributed data[30] (which was the case here for the AMS measurements) and was propagated from the uncertainties associated with the measured ^{63}Ni/Ni ratios, the measured mass of the Cu samples, the measured total Ni concentrations of the copper samples, and the measured background of ^{63}Ni atoms per g Cu in unexposed copper samples. As these are taken to be independent variables, the uncertainties were propagated in quadrature. The results show a consistent set of measurements with the ^{63}Ni atoms per g Cu values decreasing sharply with increasing distance from the bomb explosion and approaching a constant background beyond about 1,800 m (Table 1). The constant background beyond about 1,800 m appears to originate from a combination of *in situ* production of ^{63}Ni due to cosmic rays, sample processing, and AMS measurement. The next-to-last column lists the measured ^{63}Ni atoms per g Cu ratios after subtracting a background value of 7.3 $(+2.4,-1.9) \times 10^4$ atoms of ^{63}Ni per g Cu and correction for radioactive decay since 1945. Correction for radioactive decay of ^{63}Ni was done to provide comparisons with calculations at the time of bombing. Listed in the last column are the results from the sample-specific DS86 calculations at the time of bombing.

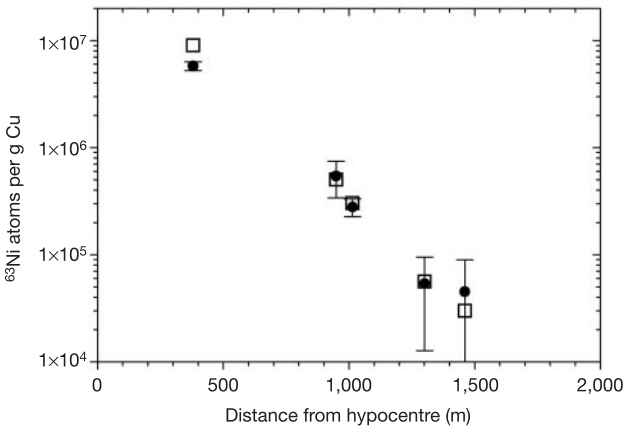

Figure 1 Measured and calculated ^{63}Ni produced in copper samples by the bomb neutrons in Hiroshima. The measured bomb-induced activation (solid circles) was obtained by first subtracting the background of 7.3×10^4 atoms ^{63}Ni per g Cu from the total measured values and then correcting for the radioactive decay of ^{63}Ni (half-life, 100.1 $\pm$ 2.0 yr) since 1945. The measurements are compared with results from sample-specific computer modelling calculations based on the DS86 dosimetry system (open squares).

These data and the results of the calculations are plotted in Fig. 1. They demonstrate that our ^{63}Ni measurements are in good agreement with those predicted from DS86 at distances between 900 and 1,500 m. This is particularly significant because that is the range of distances that dominate the atomic-bomb-survivor data and hence the radiation risk estimates for human cancer. The measurement at 380 m is somewhat below the DS86 calculation, suggesting that some downward revision in the DS86 neutron doses should be considered at distances closer to the hypocentre. The result for ^{63}Ni at 380 m has been compared with the results available for ^{32}P at similar distances. Six ^{32}P measurements at distances ranging from 331 to 433 m were obtained from an evaluation of the ^{32}P data in Hiroshima[23]. Expressing these measurements as measured-to-calculated ratios, that is, (measured ^{32}P)/(calculated ^{32}P) based on DS86, results in a mean for the six ^{32}P measurements of 0.75 with a standard deviation of 0.12. This is compared with our ^{63}Ni measurement at 380 m, which has a measured-to-calculated ratio of 0.64 $\pm$ 0.06. From this comparison it is observed that the fast neutron measurements at about 400 m from the hypocentre are in reasonable agreement with each other and both sets of measurements are lower than DS86. These results may be consistent with a slightly underestimated height-of-burst for the Hiroshima bomb.

In conclusion, good agreement of our experimental results for fast-neutron fluences with DS86 calculations is observed at the most important distances between 900 and 1,500 m. Given the close correlation between fast-neutron fluence and neutron dose, it is inferred from these results that neutron dose discrepancies, if there are any, should also be small at these distances. Taken together with previous findings that the gamma rays were adequately validated in Hiroshima and Nagasaki using thermoluminescence dosimetry (TLD)[6] and that the neutrons appear to be consistent with DS86 in Nagasaki[19], these results provide a strong measurement basis for the Hiroshima dosimetry and suggest that any future revisions in the doses for atomic-bomb survivors should be minor. □

Received 24 March; accepted 28 May 2003; doi:10.1038/nature01815.

1. BEIR V Report. *Health Effects of Exposure to Low Levels of Ionizing Radiation* (National Academy Press, Washington DC, 1990).
2. Hoshi, M. *et al.* Europium-152 activity induced by Hiroshima atomic bomb neutrons: comparison with the ^{32}P, ^{60}Co, and ^{152}Eu activities in Dosimetry System 1986 (DS86). *Health Phys.* **57,** 831–837 (1989).
3. Straume, T. *et al.* Neutron discrepancies in the DS86 Hiroshima dosimetry system. *Health Phys.* **63,** 421–426 (1992).
4. Shizuma, K. *et al.* Residual ^{152}Eu and ^{60}Co activities induced by neutrons from the Hiroshima atomic bomb. *Health Phys.* **65,** 272–282 (1993).
5. Shizuma, K. *et al.* Residual ^{60}Co activity in steel samples exposed to the Hiroshima atomic-bomb neutrons. *Health Phys.* **75,** 278–284 (1998).
6. Roesch, W. C. (ed.) *US-Japan Joint Reassessment of Atomic Bomb Radiation Dosimetry in Hiroshima and Nagasaki -Final Report* (Radiation Effects Research Foundation, Hiroshima, 1987).
7. Marchetti, A. A. *et al.* Ultra-separation of nickel from copper metal for the measurement of ^{63}Ni by AMS. *Nucl. Instrum. Meth. B* **123,** 230–234 (1997).
8. McAninch, J. E. *et al.* Measurement of ^{63}Ni and ^{59}Ni by accelerator mass spectrometry using characteristic projectile X-rays. *Nucl. Instrum. Meth. B* **123,** 137–142 (1997).
9. Knie, K., Faestermann, T. & Korschinek, G. AMS at the Munich gas-filled analyzing magnet system GAMS. *Nucl. Instrum. Meth. B* **123,** 128–131 (1997).
10. Rugel, G. *et al.* Accelerator mass spectrometry of ^{63}Ni using a gas-filled magnet at the Munich Tandem Laboratory. *Nucl. Instrum. Meth. B* **172,** 934–938 (2000).
11. Rühm, W. *et al.* Accelerator mass spectrometry of ^{63}Ni at the Munich tandem laboratory for estimating fast neutron fluences from the Hiroshima atomic bomb. *Health Phys.* **79,** 358–364 (2000).
12. Hashizume, T. *et al.* Estimation of the air dose from the atomic bombs in Hiroshima and Nagasaki. *Health Phys.* **13,** 149–161 (1967).
13. Nakanishi, T., Imura, T., Komura, K. & Sakanoue, M. ^{152}Eu in samples exposed to the nuclear explosions at Hiroshima and Nagasaki. *Nature* **302,** 132–134 (1983).
14. Haberstock, G. *et al.* Accelerator mass spectrometry with fully stripped ^{36}Cl ions. *Radiocarbon* **28,** 204–210 (1986).
15. Korschinek, G. *et al.* Accelerator mass spectrometry with completely stripped ^{41}Ca and ^{53}Mn ions at the Munich tandem accelerator. *Nucl. Instrum. Meth. B* **29,** 67–71 (1987).
16. Straume, T. *et al.* Use of accelerator mass spectrometry in the dosimetry of Hiroshima neutrons. *Nucl. Instrum. Meth. B* **52,** 552–556 (1990).
17. Kato, K. *et al.* Accelerator mass spectrometry of ^{36}Cl produced by neutrons from the Hiroshima bomb. *Int. J. Radiat. Biol.* **58,** 661–672 (1990).
18. Rühm, W., Kato, K., Korschinek, G., Morinaga, H. & Nolte, E. ^{36}Cl and ^{41}Ca depth profiles in a Hiroshima granite stone and the dosimetry system 1986. *Z. Phys. A* **341,** 235–238 (1992).
19. Straume, T., Harris, L. J., Marchetti, A. A. & Egbert, S. D. Neutrons confirmed in Nagasaki and at the Army Pulsed Radiation Facility: implications for Hiroshima. *Radiat. Res.* **138,** 193–200 (1994).

20. Rühm, W. *et al.* The dosimetry system DS86 and the neutron discrepancy in Hiroshima—historical review, present status, and future options. *Radiat. Environ. Biophys.* **37,** 293–310 (1998).
21. Arakatsu, B. *Collection of Investigative Reports on Atomic Bomb Disaster* 34–35 (Science Council of Japan, Tokyo, 1953).
22. Yamasaki, F. & Sugimoto, A. *Collection of Investigative Reports on Atomic Bomb Disaster* 18–19 (Science Council of Japan, Tokyo, 1953).
23. Gritzner, M. L. & Woolson, W. A. in *US-Japan Joint Reassessment of Atomic Bomb Radiation Dosimetry in Hiroshima And Nagasaki-Final Report* Vol. 2 (ed. Roesch, W. C.) 283–292 (Radiation Effects Research Foundation, Hiroshima, 1987).
24. Barnes, I. L., Garfinkel, S. B. & Mann, W. B. Standardization of ^{63}Ni by efficiency tracing. *Int. J. Appl. Radiat. Isot.* **22,** 781–783 (1971).
25. Marchetti, A. A. & Straume, T. A search for neutron reactions that may be useful for Hiroshima dose reconstruction. *Appl. Radiat. Isotop.* **47,** 97–103 (1996).
26. Straume, T., Marchetti, A. A. & McAninch, J. E. New analytical capability may provide solution to the neutron dosimetry problem in Hiroshima. *Radiat. Prot. Dosim.* **67,** 5–8 (1996).
27. Shibata, T. *et al.* A method to estimate the fast-neutron fluence for the Hiroshima atomic bomb. *J. Phys. Soc. Jpn* **63,** 3546–3547 (1994).
28. Johnson, J. O. (ed.) *A User's Manual for MASH v.2.0–Monte Carlo Adjoint Shielding Code System* Report ORNL/TM/11778/R2 (Oak Ridge National Laboratory, Oak Ridge, TN, 1999).
29. Rose, P. F. (ed.) *ENDF/B-VI Summary Documentation, Cross-Section Evaluation Group* Report BNL-NCS-17541 (Nuclear Data Center, Brookhaven National Laboratory, Upton, NY, 1991).
30. Feldman, G. J. & Cousins, R. D. Unified approach to the classical statistical analysis of small signals. *Phys. Rev. D* **57,** 3873–3889 (1998).

Acknowledgements We thank I. Proctor and A. M. Kellerer for their essential support of this project. We also thank S. Fujita and K. Shizuma for providing copper samples for this study. We thank the following organizations for supporting this work: the US Department of Energy, the US National Academy of Sciences, the European Commission, the German Federal Ministry of Environment, Nature Conservation and Nuclear Safety.

Competing interests statement The authors declare that they have no competing financial interests.

Correspondence and requests for materials should be addressed to T.S. (Straume1@aol.com).

Niche lability in the evolution of a Caribbean lizard community

Jonathan B. Losos[1], Manuel Leal[2]*, Richard E. Glor[1], Kevin de Queiroz[3], Paul E. Hertz[4], Lourdes Rodríguez Schettino[5], Ada Chamizo Lara[5], Todd R. Jackman[6] & Allan Larson[1]

[1]*Department of Biology, Campus Box 1137, Washington University, St. Louis, Missouri 63130, USA*
[2]*Department of Biological Sciences, Union College, Schenectady, New York 12308, USA*
[3]*Division of Amphibians and Reptiles, National Museum of Natural History, Smithsonian Institution, Washington, DC 20560, USA*
[4]*Department of Biology, Barnard College, 3009 Broadway, New York 10027, USA*
[5]*Instituto de Ecología y Sistemática, CITGMA, Carretera de Varona km 3.5, Boyeros, La Habana 10800, Apartado Postal 8029, Cuba*
[6]*Department of Biology, Villanova University, Villanova, Pennsylvania 19085, USA*

* Present address: Department of Biological Sciences, Vanderbilt University, VU Station B 351634 Nashville Tennesee 37235, USA

Niche conservatism—the tendency for closely related species to be ecologically similar—is widespread[1–3]. However, most studies compare closely related taxa that occur in allopatry[3]; in sympatry, the stabilizing forces that promote niche conservatism[4,5], and thus inhibit niche shifts, may be countered by natural selection favouring ecological divergence to minimize the intensity of interspecific interactions[6,7]. Consequently, the relative importance of niche conservatism versus niche divergence in determining community structure has received little attention[7]. Here, we examine a tropical lizard community in which species have a long evolutionary history of ecological interaction. We find that evolutionary divergence overcomes niche conservatism: closely related species are no more ecologically similar than expected by random divergence and some distantly related species are ecologically similar, leading to a community in which the relationship between ecological similarity and phylogenetic relatedness is very weak. Despite this lack of niche conservatism, the ecological structuring of the community has a phylogenetic component: niche complementarity only occurs among distantly related species, which suggests that the strength of ecological interactions among species may be related to phylogeny, but it is not necessarily the most closely related species that interact most strongly.

Anolis lizards are a dominant component of Caribbean ecosystems (reviewed in refs 8 and 9) and are well suited for studies of the evolution of community structure because the species on individual islands have a long history of interaction and coevolution. For example, 55 of 58 species on Cuba are endemic (the remaining three have colonized other Caribbean islands from Cuba), and most are members of large clades that have diversified on Cuba[10]. Species on many islands attain extremely high densities[11,12], and many species—differing in ecology, morphology, and behaviour—coexist locally[8]. Interactions among sympatric species can be strong[8,9,13,14], usually as a result of interspecific competition, although intra-guild predation may sometimes be important[15].

We studied the community structure of anoles at Soroa, Biosphere Preserve Sierra del Rosario, in the Pinar del Río province of western Cuba. Eleven anole species occur sympatrically at Soroa, the highest anole diversity known from any island or continental site. Of these species, ten are either widely distributed in Cuba or are members of island-wide clades of ecologically similar species (for example, the *Anolis equestris* group, to which *A. luteogularis* belongs, occurs throughout Cuba and is composed of six primarily allopatric species similar in morphology and ecology). Because the clades of Cuban anoles to which the Soroa species belong are widespread and arose within a relatively short period in the distant past[10] (Fig. 1), the sympatric clades at Soroa have probably coexisted for a long time and over a large spatial scale. Thus, these *Anolis* species probably evolved in the presence of the same clades with which they currently coexist, a necessary prerequisite for community coevolution.

We examined ecological relationships among these species to investigate whether the community exhibited nonrandom ecological or phylogenetic structure. We measured ecological variables relevant to the three resource axes that sympatric *Anolis* generally partition: structural habitat, thermal habitat, and prey size[16]. Principal components analysis reveals three significant axes of ecological differentiation (Table 1; results below are qualitatively unchanged if another, nearly significant, axis is also retained). Examination of the position of species in multivariate ecological space reveals both that niche use has not been conserved and that the community is nonrandomly structured (Fig. 2).

The minimal extent of niche conservatism is indicated by the weak association between phylogenetic relationship and position in multivariate ecological space: phylogenetic similarity explains less than 4% of the variation in ecological similarity among species (Mantel test, $P = 0.11$–0.30 depending on phylogenetic topology and mode of character evolution used in the analysis; all variables but one exhibit similarly low correlations with phylogenetic relationships (Table 1); *P*-values in Mantel tests based on 5,000 simulations). The molecular data strongly reject alternative phylogenetic topologies in which ecologically similar species are grouped phylogenetically (see Supplementary Information).

Although some closely related species differ little ecologically, many distantly related species are just as ecologically similar, and some closely related species are ecologically dissimilar (Fig. 2). Moreover, although members of the *sagrei* and *porcatus* clades form clusters in ecological space (Fig. 2; multivariate analysis of variance, MANOVA, Wilks' $\lambda = 0.013$, $F_{12,10} = 3.79$, $P = 0.018$), they are no more ecologically similar than would be expected for

